Electronic Supplementary Information

A porphyrin-triazatruxene dyad for ratiometric two-photon fluorescent sensing of intracellular viscosity

Yi Wang, Tong Lei, Jinghui Zhang, Lei Gong, Yanjie Yang, Xiaolin Ma, Yongqiang Wen, Hongwu Du, Dongdong Qi, Yongzhong Bian, Zhiqiang Liu and Jianzhuang Jiang

Content

1. Chemicals and Instruments

All reagents were used directly as obtained commercially unless otherwise noted. Column chromatography was carried out on silica gel (200-300 mesh, Qingdao Ocean Chemicals) and Bio-beads (200-400 mesh, BIORAD S-X1) with the indicated eluents. CH_2Cl_2 and Et_3N were freshly distilled from CaH_2 under N_2. THF was freshly distilled from Na under N_2.

^{1}H NMR spectra were recorded on a Bruker DPX 400 MHz spectrometer in deuterated chloroform ($CDCl_3$), deuterated tetrahydrofuran (THF-d_8) or deuterated dimethyl sulfoxide (DMSO-d_6) and the chemical shifts (δ, ppm) were reported relative to tetramethylsilane ($SiMe_4$). MALDI-TOF mass spectra were measured on a Bruker Microflex™ LRF spectrometer with dithranol as the matrix. Elemental analyses were performed on an Elementar Vario MICRO CUBE elemental analyzer. Electronic absorption spectra were recorded on a Lambda U-750 spectrophotometer. Steady-state fluorescence spectra were acquired on a FLS980 spectrofluorimeter (Edinburgh). All fluorescence spectra were measured in a quartz cell with 10 mm optical length. A 375 nm laser (EPL) was used as exciting source to measure the fluorescence lifetimes. The two-photon fluorescence emission spectra were measured on a SpectroPro300i spectrameter using the pump laser beam came from a mode-locked Ti:sapphire laser system (Coherent) at the pulse duration of 220 fs, a repetition rate of 76 MHz. The wavelength of the output laser beam was tuned from 730 to 890 nm.

2. Synthesis and Characterization
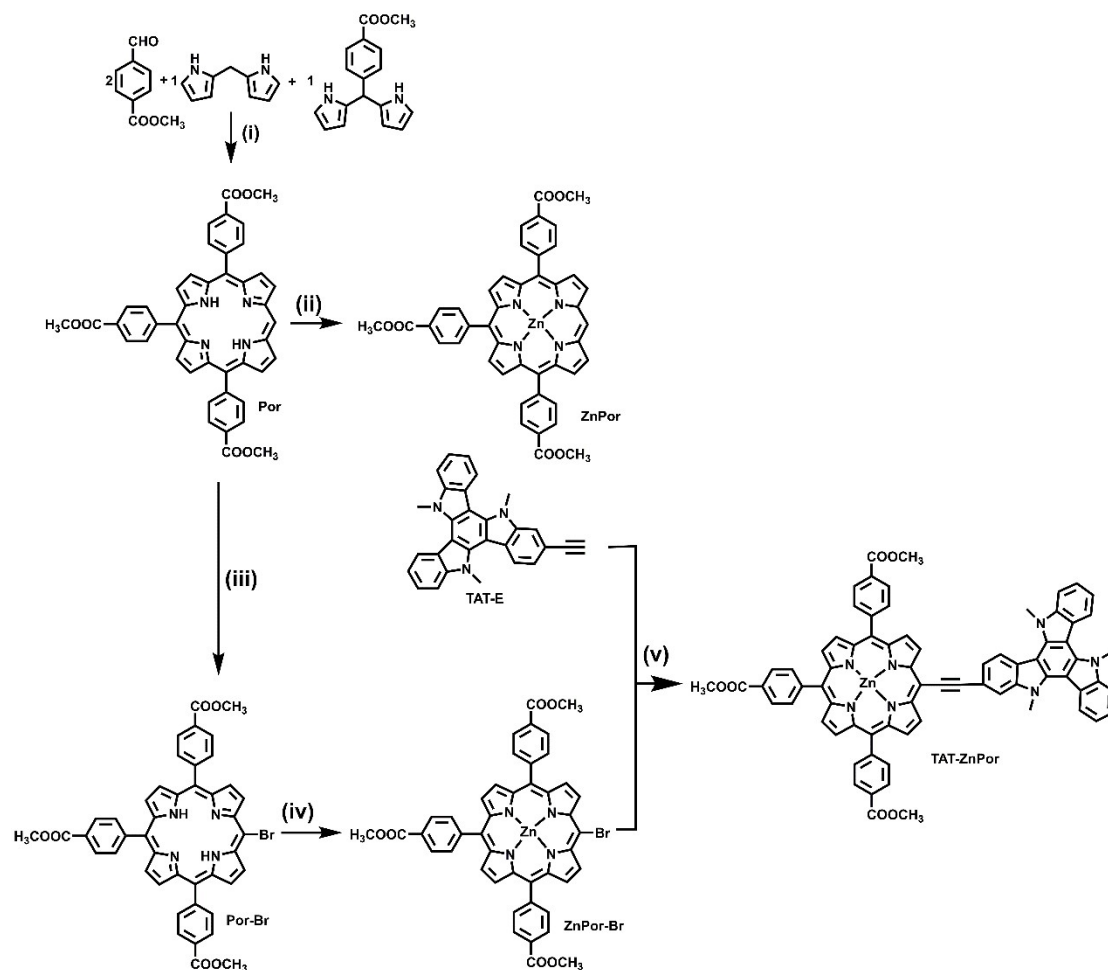
Scheme S1 Synthesis of porphyrin derivaties: (i) TFA, DDQ, CH$_2$Cl$_2$, 25 °C; (ii) Zn(OAc)$_2$, CHCl$_3$/CH$_3$OH, reflux; (iii) NBS, CH$_2$Cl$_2$, 0 °C; (iv) Zn(OAc)$_2$, CHCl$_3$/CH$_3$OH, reflux; (v) Pd(pph$_3$)$_2$Cl$_2$, CuI, THF/Et$_3$N, 50 °C.

Synthesis of **Por.** To a freshly distilled CH$_2$Cl$_2$ (700 mL) containing methyl 4-formylbenzoate (1.53 g, 9.30 mmol), dipyrromethane (682 mg, 4.67 mmol), and 4-dipyrrole methyl benzoate (1.31 g, 4.67 mmol) was added TFA (420 uL, 5.60 mmol). The mixture was stirred for 4 h at 25 °C under N$_2$ atmosphere. DDQ (3.13 g, 14 mmol) was added, and the mixture was stirred for 3 h. The crude product was purified by silica gel column with CH$_2$Cl$_2$ as the eluent, where the second fraction was collected and further recrystallized with CH$_2$Cl$_2$/ CH$_3$OH to afforded compound **Por** (256 mg, 7.7%) as purple solid. ^{1}H NMR (DMSO, 400 MHz, 293K): δ 10.62 (s, 1H), 9.65 (d, J = 4.64

3

Hz, 2H), 8.99 (d, J = 4.64Hz, 2H), 8.98 (m, 2H), 8.84 (m, 2H), 8.38(m, 12H), 4.06 (s, 9H), -3.19 (s, 2H). MALDI-TOF-MS: m/z calcd for $C_{44}H_{32}N_4O_6$ [M]$^+$ 712.23; found 712.59. Anal. calcd for $C_{44}H_{32}N_4O_6\cdot H_2O$: C, 72.32%; H, 4.69%; N, 7.67%. Found: C, 72.36%; H, 4.93%; N, 7.41%.

Synthesis of **ZnPor.** To a solution of zinc acetate (50 mg, 0.27 mmol) in $CHCl_3/CH_3OH$ (v:v, 2:1) 24 mL, porphyrin **Por** (17.5 mg, 0.025 mmol) was added. After refluxing for 2 h, the solvent was removed under reduced pressure and the residue was purified on a silica gel column using CH_2Cl_2 as the eluent, and further recrystallized with CH_2Cl_2/ n-hexane to afforded compound **ZnPor** (18 mg, 93%) as purple solid. ^{1}H NMR (CDCl$_3$, 400 MHz, 293K): δ 10.33 (s, 1H), 9.44 (d, J = 4.34 Hz, 2H), 9.07 (d, J = 4.34 Hz, 2H), 8.95 (m, 4H), 8.46 (s, 6H), 8.33 (m, 6H), 4.12 (m, 9H). MALDI-TOF-MS: m/z calcd for $C_{44}H_{30}N_4O_6Zn$[M]$^+$ 774.16; found 774.18. Anal. calcd for $C_{44}H_{30}N_4O_6Zn\cdot 2.5H_2O$: C, 64.36%; H, 4.30%; N, 6.82%. Found: C, 64.37%; H, 4.25%; N, 6.73%.

Synthesis of **Por-Br.** To a solution of **Por** (240 mg, 0.34 mmol) in CH_2Cl_2 (50 mL), NBS (60 mg, 0.34 mmol) was added dropwise in 30 min at 0 ℃. After the mixture was stirred for another 1 h, the solvent was removed in vacuum. The residual was then purified on a silica gel columns using CH_2Cl_2/ n-hexane (v:v, 3:1) as the eluent and further recrystallized with CH_2Cl_2/ CH_3OH to afforded **Por-Br** (205 mg, 77%) as purple solid. ^{1}H NMR (CDCl$_3$, 400 MHz, 293K): δ 9.71 (d, J = 4.4 Hz, 2H), 8.78 (d, J = 4.4 Hz, 2H), 8.76 (m, 4H), 8.45 (s, 6H), 8.26 (m, 6H), 4.13 (m, 9H), -2.71 (s, 2H). MALDI-TOF-MS: m/z calcd for $C_{44}H_{31}BrN_4O_6$[M]$^+$ 790.14; found 792.09. Anal. calcd for $C_{44}H_{31}BrN_4O_6\cdot H_2O$: C, 65.27%; H, 4.11%; N, 6.92%. Found: C, 66.47%; H, 4.51%; N, 6.75%.

Synthesis of **ZnPor-Br.** To a solution of zinc acetate (500 mg, 2.70 mmol) in $CHCl_3$/methanol (v:v, 2:1) 150 mL, porphyrin **Por-Br** (193 mg, 0.24 mmol) was added. After refluxing for 2 h, the solvent was removed under reduced pressure and the residue

was purified on a silica gel column using CH_2Cl_2/n-hexane (v:v, 4:1) as the eluent, and further recrystallized with CH_2Cl_2/ CH_3OH to afforded compound **ZnPor-Br** (176 mg, 83%) as purple solid. ^{1}H NMR ($CDCl_3$, 400 MHz, 293K): δ 9.79 (d, J = 4.75 Hz, 2H), 8.94 (d, J = 4.75 Hz, 2H), 8.85 (m, 4H), 8.42 (s, 6H), 8.27 (d, J = 4.0 Hz, 6H), 4.10(m, 9H). MALDI-TOF-MS: m/z calcd for $C_{44}H_{29}BrN_4O_6Zn[M]^+$ 854.07; found 854.04.

Anal. calcd for $C_{44}H_{29}BrN_4O_6Zn \cdot 1.5H_2O$: C, 59.91%; H, 3.66%; N, 6.35%. Found: C, 59.92%; H, 3.65%; N, 5.86%.

3. Experimental Methods

Quantum yield measurement. Fluorescence quantum yields of **TAT-E**, **ZnPor** and **TAT-ZnPor** were determined. The quantum yield was calculated using the following equation:

$$\Phi_x = \Phi_s(A_s F_x\, n_x^2) / (A_x F_s\, n_x^2)$$

Where Φ is the fluorescence quantum yield, A is the absorbance at the excitation wavelength, F is the area under the corrected emission curve, and n is the refractive index of the solvents used. Subscripts s and x refer to the standard and to the sample respectively. Herein, the absorption at the excitation wavelength was kept below 0.05.

Two-photon absorption cross section measurement. The two-photon excited fluorescence (TPEF) method was used to measure the TPA cross-sections (δ_{TPA}). Samples were dissolved in THF at the concentration of 2×10^{-6} M and the two-photon induced fluorescence intensity was measured at 730-890 nm by using Rhodamine B (2×10^{-6} M in methanol) as the reference.[1,2] The intensities of the two-photon-induced fluorescence spectra of the reference and samples under the same measurement conditions were determined and compared. The TPA cross-section of samples, measured by using the two-photon-induced fluorescence measurement technique, can be calculated by using the following equation:

$$\delta_s = \delta_r(F_s \Phi_r C_r n_r) / (F_r \Phi_s C_s n_s)$$

where the subscripts s and r stand for the sample and reference molecules, respectively. F is the integral area of the two-photon fluorescence; Φ is the fluorescence quantum yield; and C is the number density of the molecules in solution. δ_r is the TPA cross-section of the reference molecule; n is the refractive indices of the solvent. The measurements were conducted in a regime where the fluorescence signal showed a quadratic dependence on the excitation intensity, as expected for two-photon-induced emission.

DFT calculation. The density functional theory (DFT) and time-dependent density

functional theory (TD-DFT)[3] calculations were performed on the level of PBE0[4]/BS using Gaussian 09 D.01 software package.[5] The BS donates a mixed basis set including 6-311G(d) for C/H/N atoms and SDD for Zn atom.[6] Besides, the built-in PCM model was used to simulate the tetrahydrofuran (THF) solution environment.[7] Firstly, the π-LOL calculation were carried out using Multiwfn program,[8] which is a function for locating high-localization regions of π orbitals. When the isovalue of the surface is 0.2, both strong and weak π bonds are displayed. The results of TD-DFT calculation were further processed by TD-Analy 1.13.[9]

Cell Culture. A549 cells were incubated in DMEM containing 10% fetal bovine serum and 100 U/mL penicillin and 100 U/mL streptomycin at 37 °C in a humidified environment containing 5% CO_2. Before the experiment, the cells were precultured until confluence was reached. Stock solutions of the test compounds (1 mM) were prepared in DMSO and stored in the dark at -20 °C. These compounds were diluted to a working solution (2 μM) with DMEM when used in the fluorescence imaging.

MTT assay. A549 cells were seeded into a 96-well plate at 37 °C in a humidified incubator containing 5% CO_2 for 24 h. Then the cells were incubated with different concentrations of **TAT-ZnPor** (0, 2, 4, 8 and 16 μM) in culture medium for 30 min, respectively. The cells were washed with PBS for twice and cultured with fresh DMEM for another 24 h. Then 20 μL MTT solution (5 mg/mL) was added to each well. About 4 h later, the remaining MTT solution was carefully removed, and 150 μL DMSO was added to each well to dissolve the formed formazan crystals. After gentle agitation for 10 min, the absorbance at 492 nm was measured using the Tecan Sunrise[TM] microplate reader. The cell viability rate (V_R) was calculated according to the equation:

$$V_R = A/A_0 \times 100\%$$

where A is the absorbance of the experimental group (the cells were treated by **TAT-ZnPor** with different concentration, respectively) and A_0 is the absorbance of the control group (the cells were treated by DMEM without dyes).

One-Photon and Two-Photon Cellular Imaging. A549 cells were grown on glass-

bottom culture dishes in Dulbecco's modified eagle media supplemented with 10% (v/v) fetal bovine serum, penicillin (100 μg/mL), and streptomycin (100 μg/mL) at 37 °C in a 5% CO_2 incubator. Cells were treated with **TAT-ZnPor** (2 μM in DMEM) for 30 min and then washed with PBS solution to remove the excess **TAT-ZnPor**. Fluorescence imaging experiments were performed at 37 °C on a Nikon A1RSi$^+$ confocal laser scanning microscope with live cell imaging system and excitation at 405 nm, 457 nm (for one-photon excitation) or 820 nm (for two-photon excitation) through 60× oil immersion objective lens.

Co-localization fluorescence imaging. A549 cells were incubated with **TAT-ZnPor** (2 μM in DMEM, with 0.2% DMSO) at 37 °C for 30 min, and then stained with DilC18(3) (1 μM), MitoLite Blue FX 490 (20 μM), LysoTracker Blue DND-22 (100 nM), ER-tracker Blue-White DPX (100 nM) or ActinBlue (50 U/mL) for another 20 min. Before fluorescence imaging, the adherent cells were further washed twice with PBS (pH = 7.4) to remove the excess dyes. Fluorescence imaging experiments were performed on a LeicaSP8 confocal laser scanning microscope through 100× objective lens. Four color channels were used for these experiments: red channel (λ_{ex} = 405 nm, λ_{em} = 550-700 nm) and green channel (λ_{ex} = 405 nm, λ_{em} = 500-550 nm) for **TAT-ZnPor**, blue channel (λ_{ex} = 405 nm, λ_{em} = 400-500 nm) for MitoTracker Blue FX 490 LysoTracker Blue DND-22, ER-tracker Blue-White DPX (100 nM), ActinBlue (50 U/mL), and orange channel (λ_{ex} = 552 nm, λ_{em} = 550-600 nm) for DilC18(3).

Cell viscosity detection. A549 cells were stained with DMEM containing **TAT-ZnPor** (2 μM) for 30 min at 37 °C in a 5% CO_2 incubator, then the adherent cells were washed with PBS (pH = 7.4) to remove the excess **TAT-ZnPor**. The cells were further incubated 20 min in the presence of 100 nM nystatin or monensin. Fluorescence imaging experiments were performed on a Leica SP8 confocal microscope through 60× objective lens. Upon the excitation of 405 nm, the green channel images (500-550 nm) and the red channel images (550-700 nm) were collected, respectively.
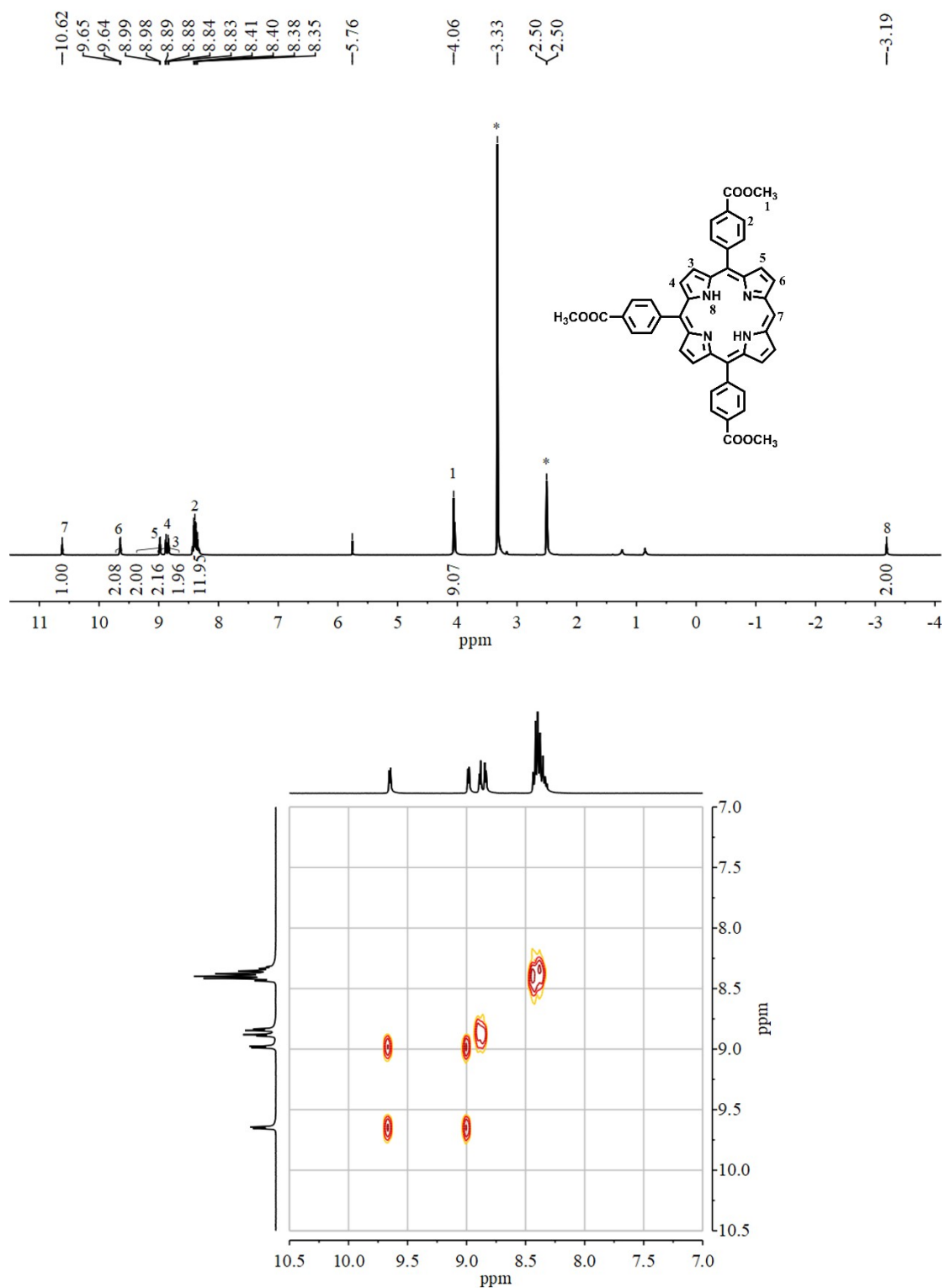
4. NMR and MALDI-TOF MS Spectra

Fig. S1 ^{1}H and ^{1}H-^{1}H COSY NMR spectra of the compound **Por** in DMSO-d_6 at 293 K.* indicate the residual solvent signals.
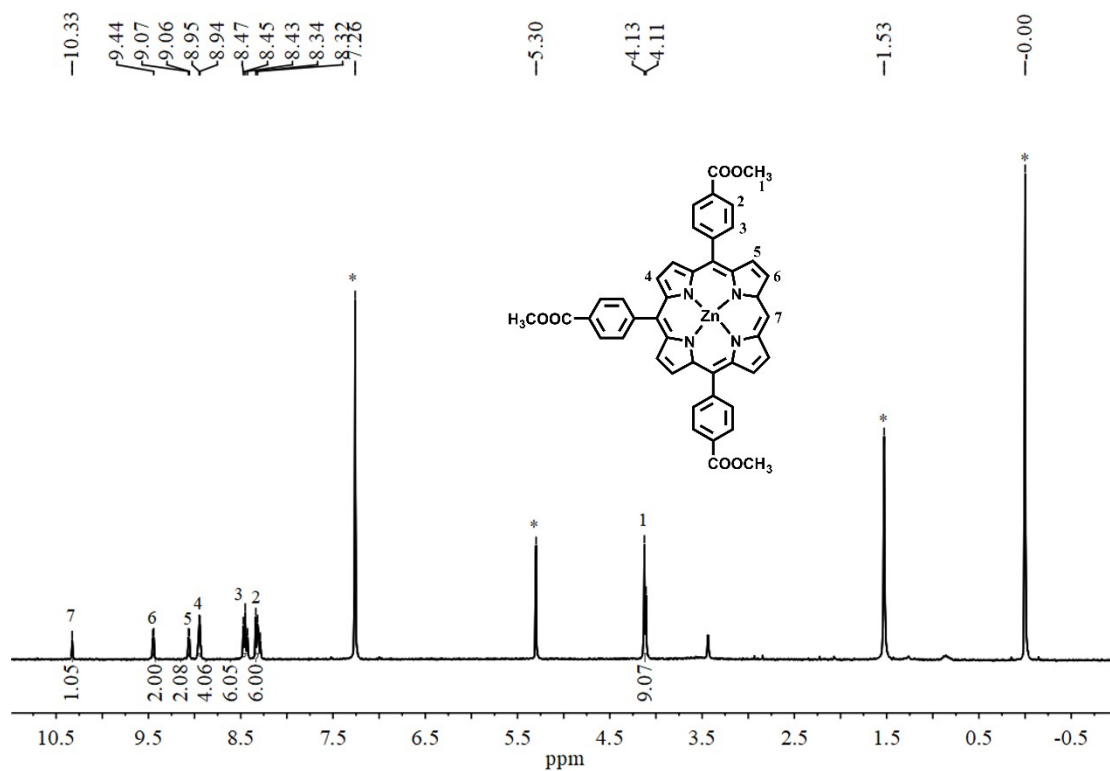
Fig. S2 ^{1}H NMR spectrum of the compound **ZnPor** in CDCl$_3$ at 293 K. * indicate the residual solvent signals.
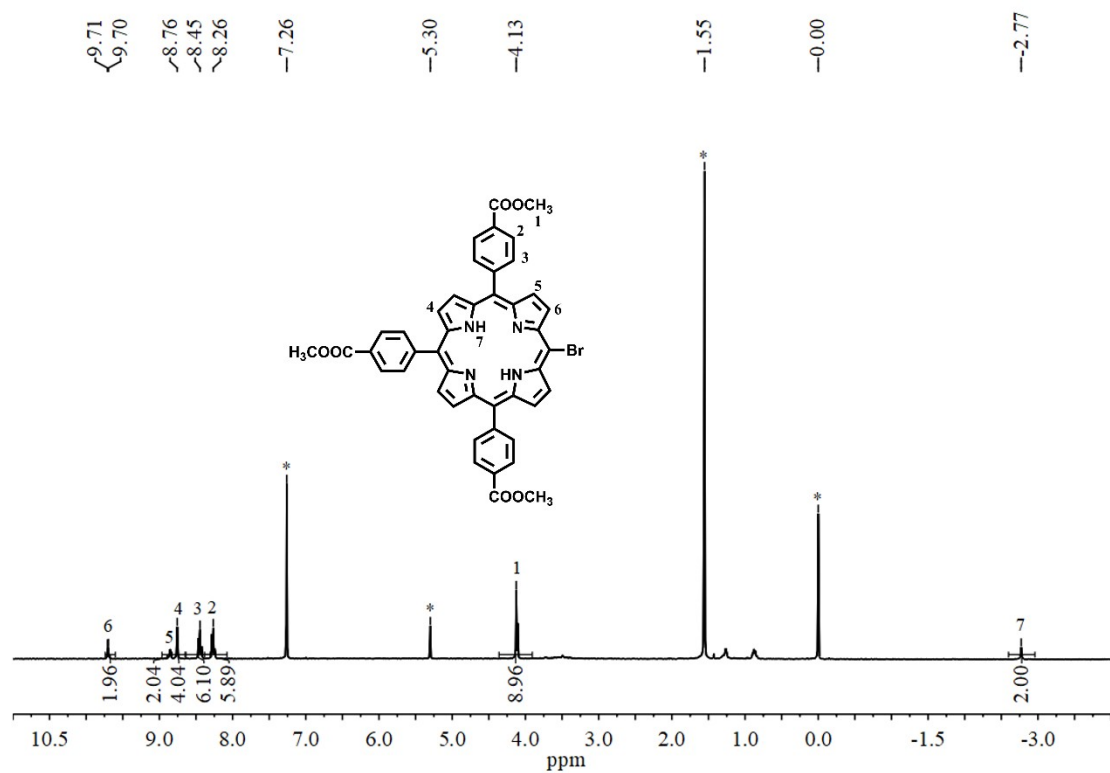
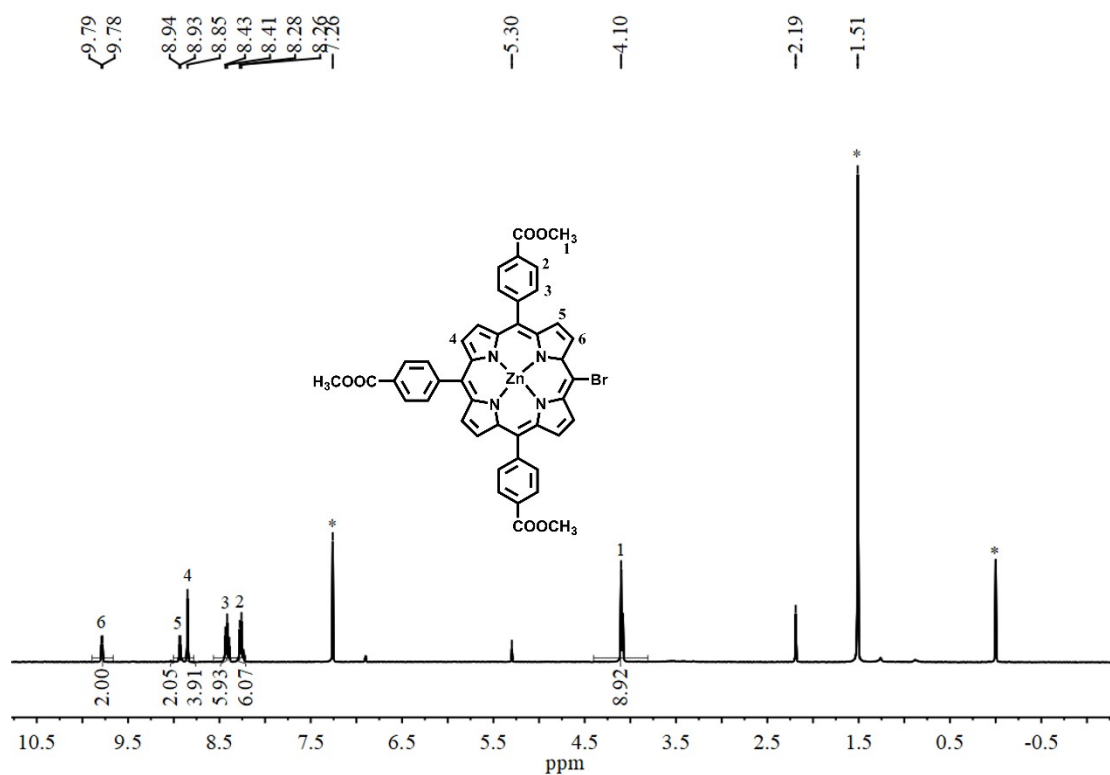**Fig. S3** ^1H NMR spectrum of the compound **Por-Br** in CDCl₃ at 293 K.* indicate the residual solvent signals.
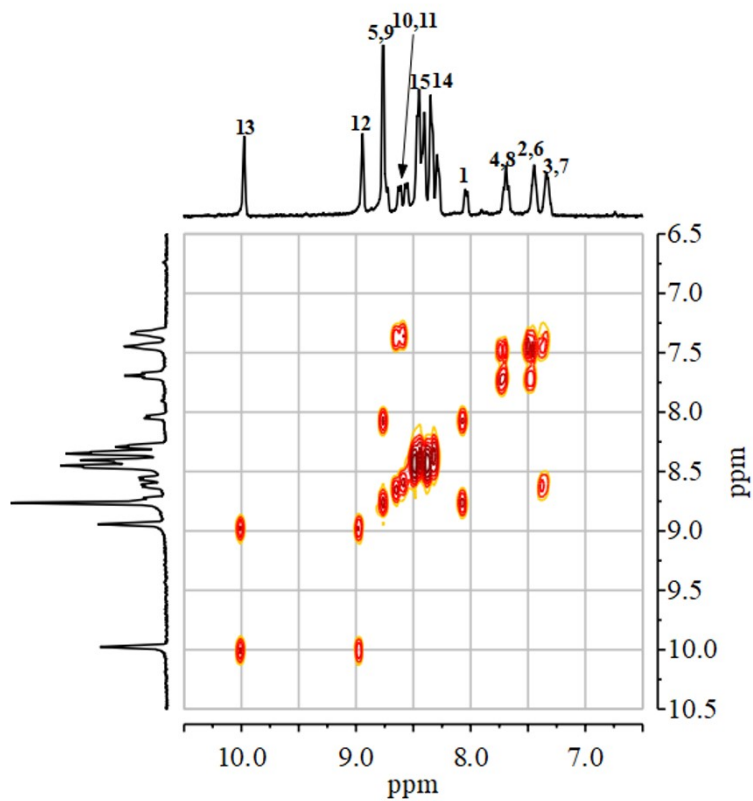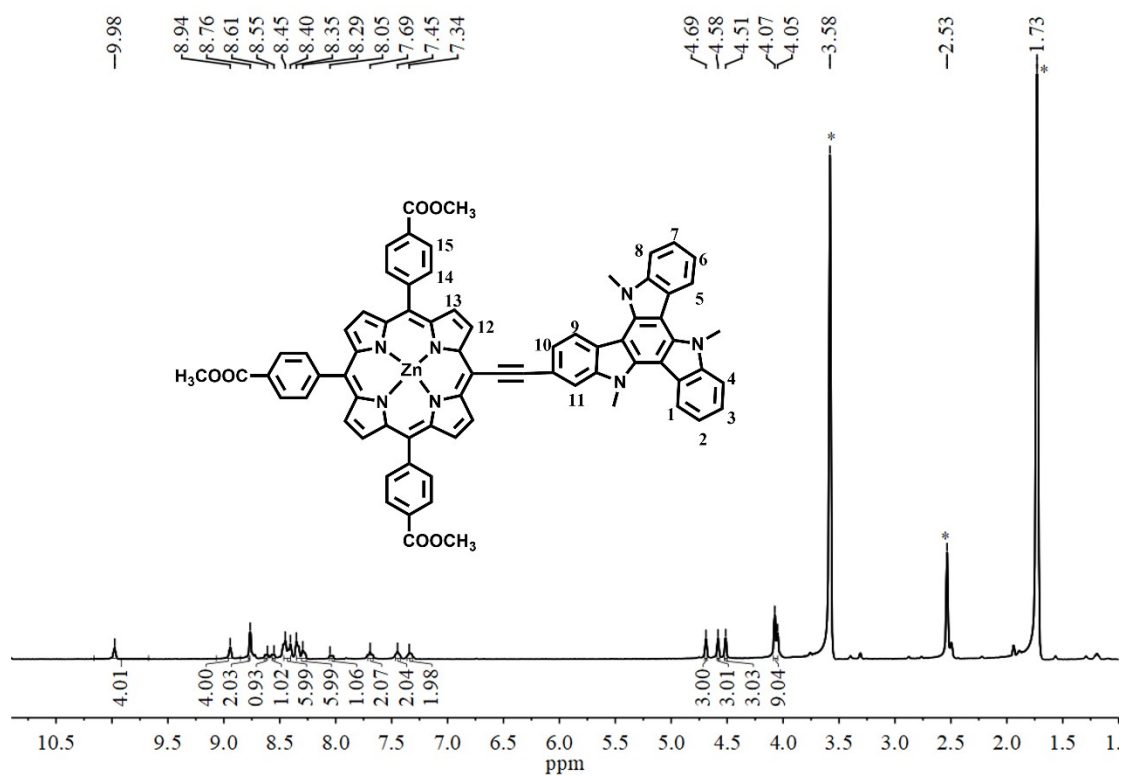
Fig. S4 ^{1}H NMR spectrum of the compound **ZnPor-Br** in CDCl$_3$ at 293 K.* indicate the residual solvent signals.

Fig. S5 ^{1}H and ^{1}H-^{1}H COSY NMR spectra of the compound **TAT-ZnPor** in THF-d_8 at 293 K.* indicate the residual solvent signals.
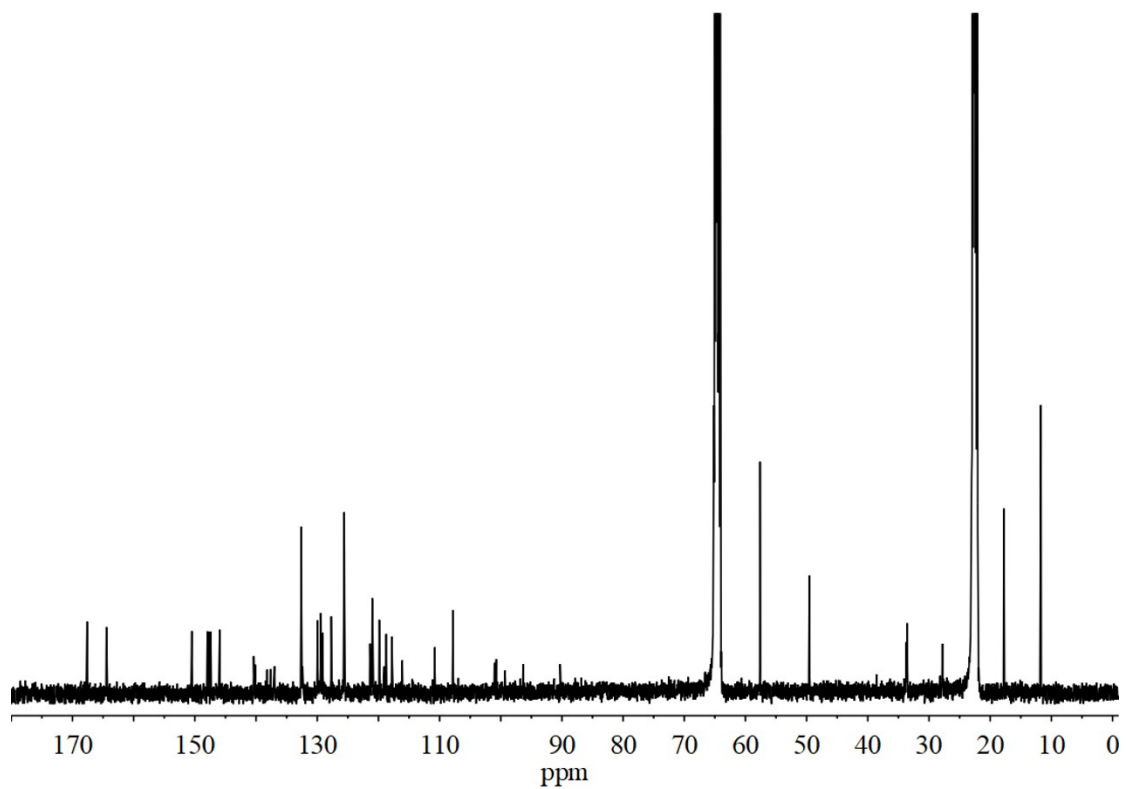
Fig. S6 ^{13}C NMR spectrum of the compound **TAT-ZnPor** in THF-d_8 at 293 K.* indicate the residual solvent signals.
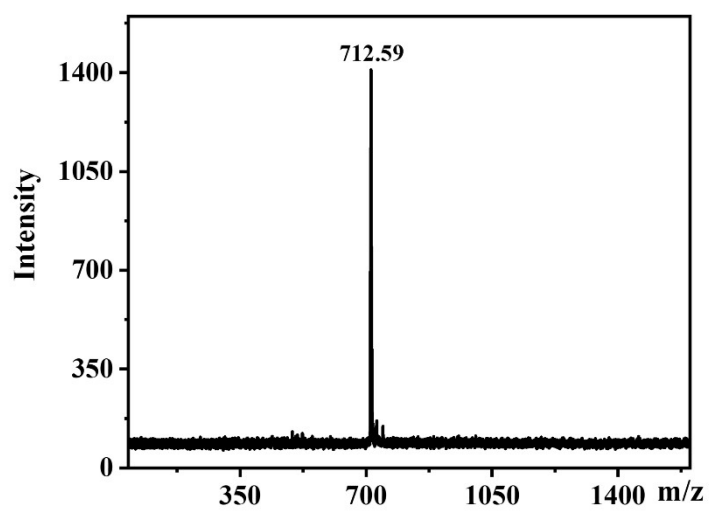
Fig. S7 MALDI-TOF mass spectrum of **Por**.

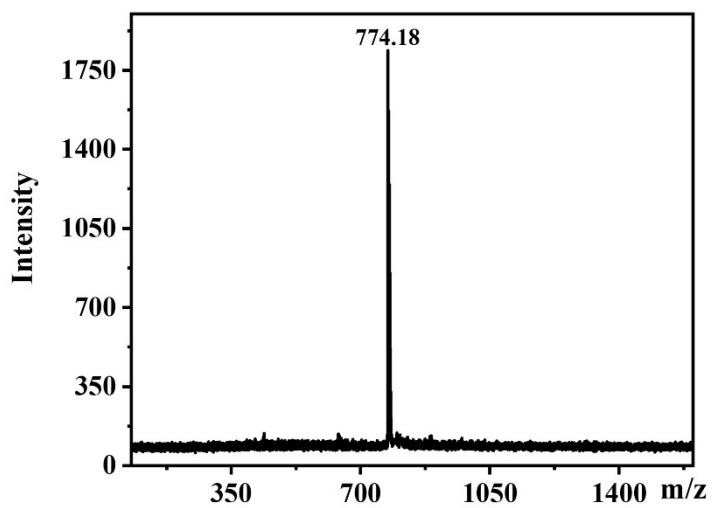
Fig. S8 MALDI-TOF mass spectrum of **ZnPor**.
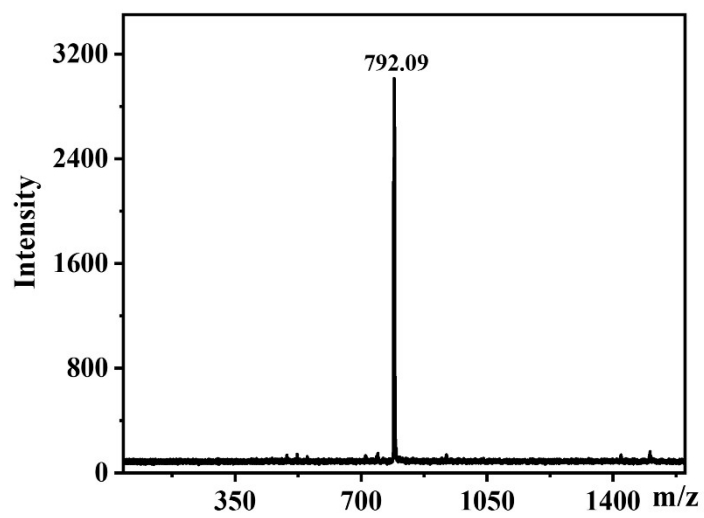
Fig. S9 MALDI-TOF mass spectrum of **Por-Br**.
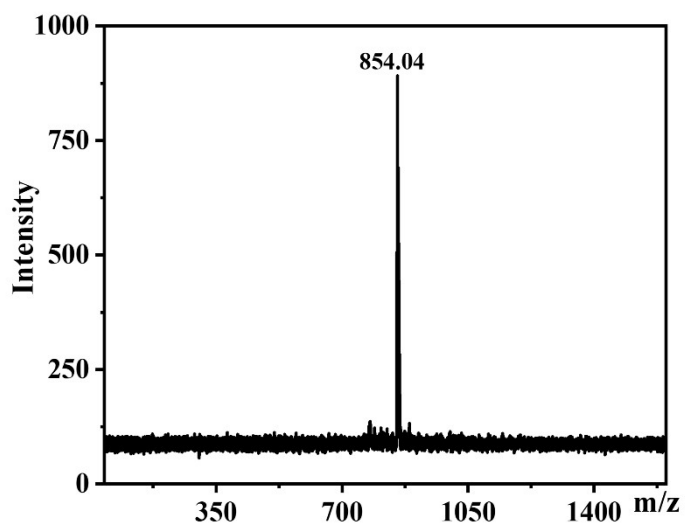
Fig. S10 MALDI-TOF mass spectrum of **ZnPor-Br**.
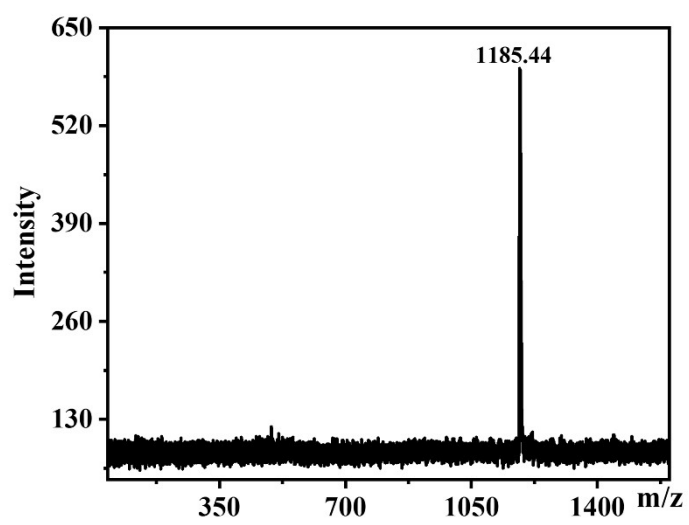
Fig. S11 MALDI-TOF mass spectrum of **TAT-ZnPor**.

5. Absorption and Fluorescent Emission Data
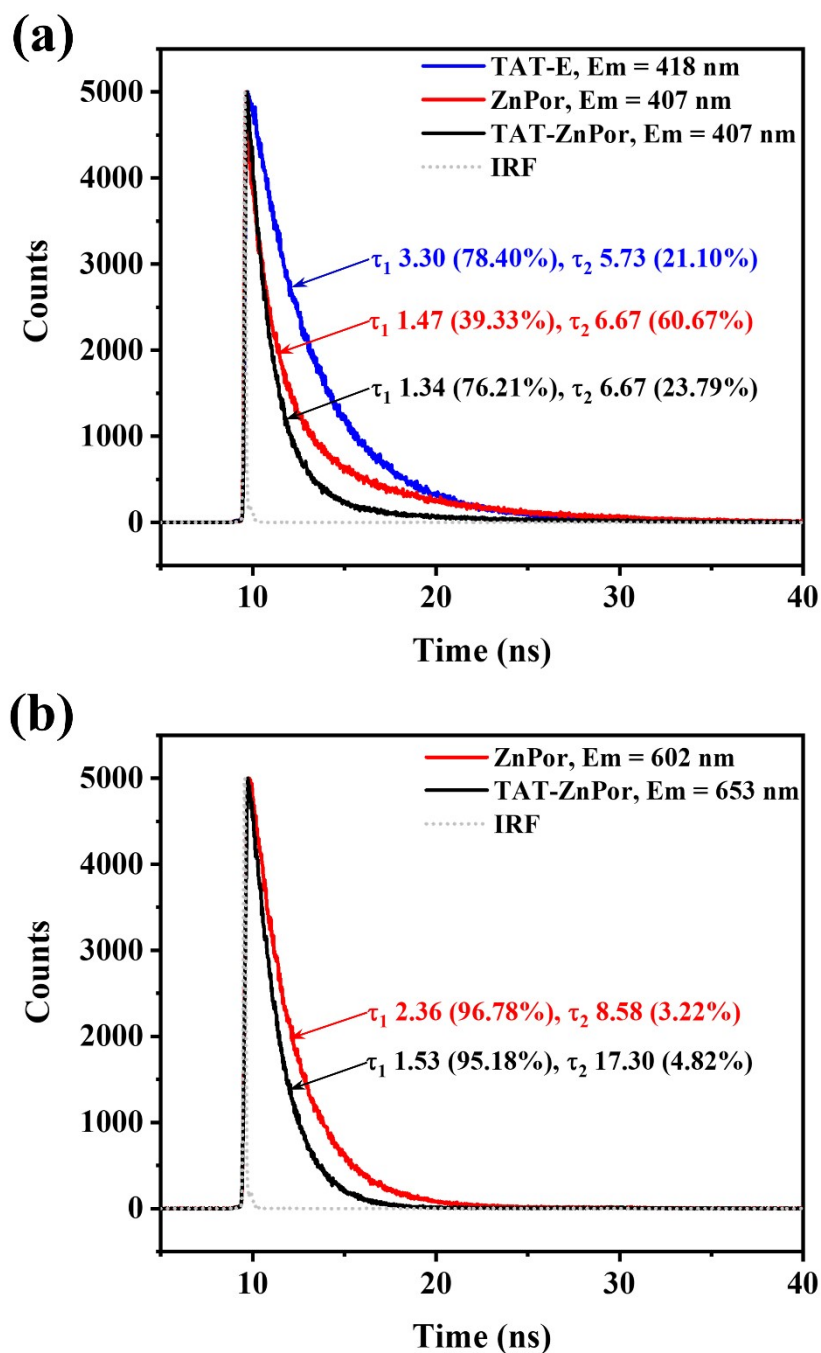
Fig. S12 Fluorescence decay curves of **TAT-E**, **ZnPor** and **TAT-ZnPor** (2 μM) at (a) blue-green emission band and (b) red emission band. The time profiles of fluorescence decays were obtained with excitation at 375 nm by a EPL laser. Dotted line is the instrument response function (IRF) of the system.

Fig. S13 (a) Absorption and (b) Fluorescence emission spectra of **TAT-ZnPor** in different solvents (1 μM, λ_{ex} = 350 nm).

Table S1 Photophysical data of **TAT-E**, **ZnPor** and **TAT-ZnPor** in THF.

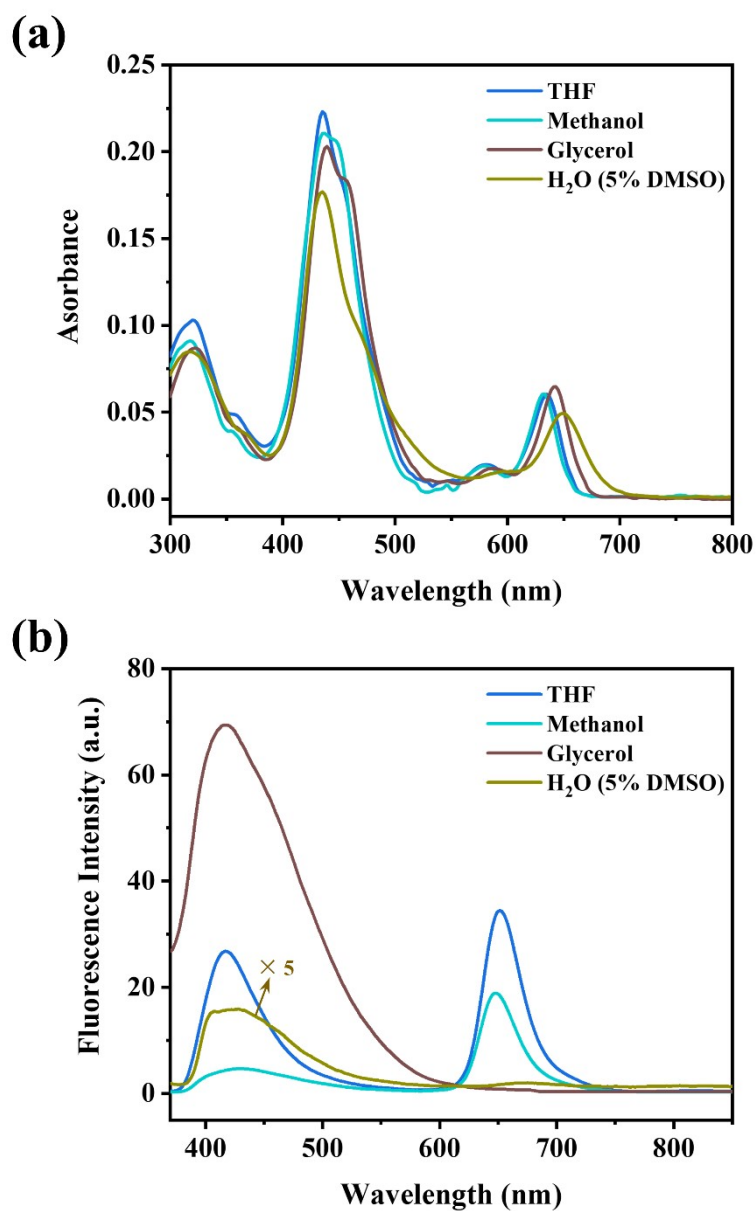|	Absorption λ_{max} [nm] Log ε (M^{-1} cm^{-1})					Emission λ_{max} [nm][a] (Φ_{em})[b] $(\tau_1, \tau_2$ [ns])[c]		δ_{TPA}	$\Phi_{em}\delta_{TPA}$[g]
TAT-E	319 (5.08)					418 (0.19) (3.30, 5.73)		53[d]	11
ZnPor	314 (4.44)	420 (5.83)	550 (4.44)	590 (3.79)		407, 446 (0.013) (1.47, 6.67)	602 (0.20) (2.36, 8.58)	17[e]	3.4
TAT-ZnPor	323 (4.98)	436 (5.50)	454 (5.34)	582 (4.30)	637 (4.80)	407 (0.021) (1.34, 6.67)	653 (0.40) (1.53, 17.30)	811[f]	324

[a]Excitation wavelength:350 nm.

[b]Fluorescence quantum yields were determined by reference to quinine sulfate in 0.1 M H_2SO_4 ($\Phi = 0.54$)[10] upon excitation at 350 nm.

[b]Fluorescence quantum yields were determined by reference to H_2TPP in toluene ($\Phi = 0.13$)[11] upon excitation of 420 nm.

[c]The fluorescence lifetimes were measured with 375 nm EPL laser excitation in THF.

[d]Two-photon cross section (GM:$10^{-50}cm^4$s/photon) at 740 nm.

[e]Two-photon cross section at 810 nm.

[f]Two-photon cross section at 820 nm.

[g]Two-photon action cross section ($\Phi_{em}\delta_{TPA}$).
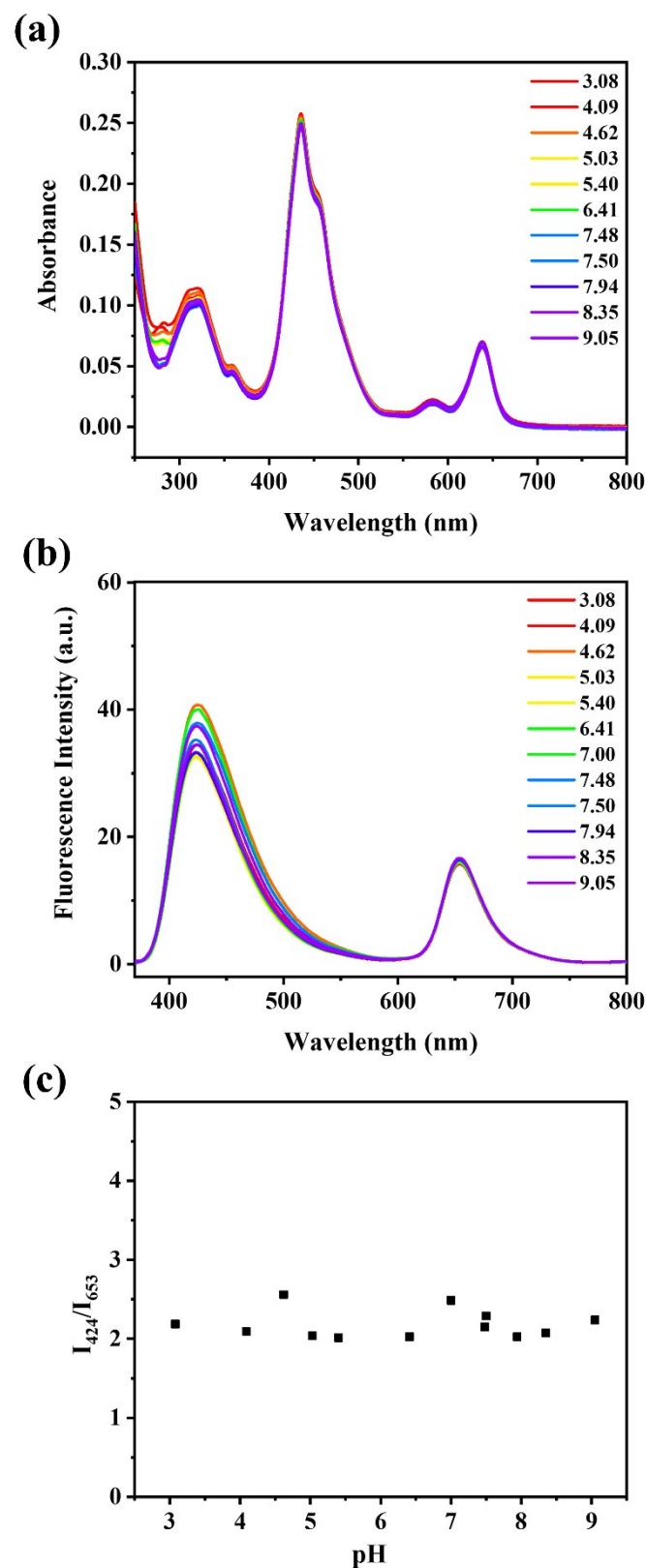
Fig. S14 (a) Absorption and (b) Fluorescence emission spectra of **TAT-ZnPor** in different pH values (pH = 3-9, V_{THF}: V_{Water} = 1:1); (c) Plots of intensity ratio (I_{424}/I_{653}) *vs.* pH value (1 μM, λ_{ex} = 350 nm).
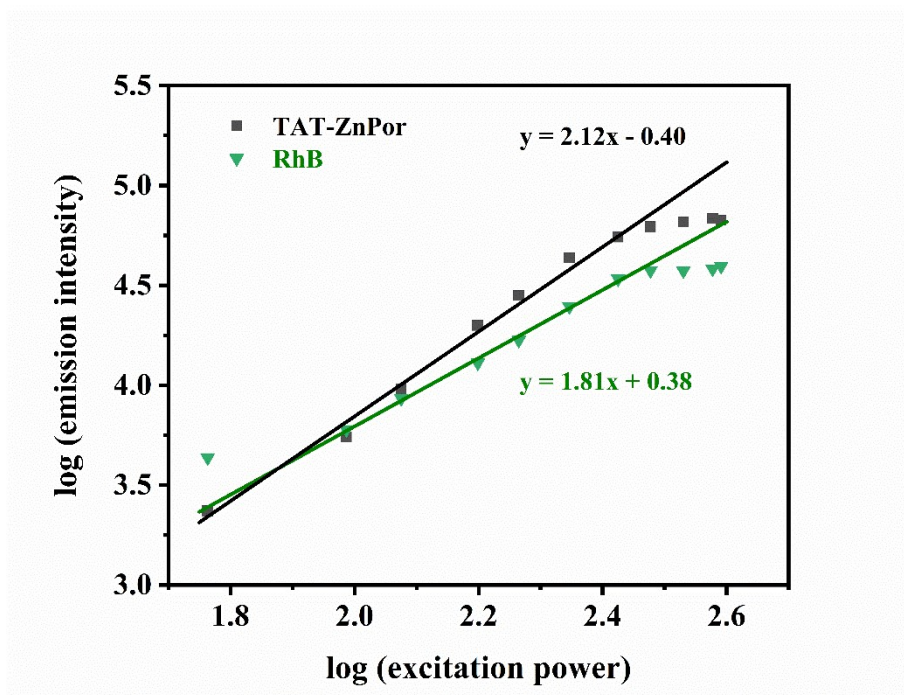
Fig. S15 Power dependence plots of the fluorescence intensity of **TAT-ZnPor** (in THF) and RhB (in CH$_3$OH) upon excitation at 800 nm (220 fs, 76 Hz).

6. DFT calculation
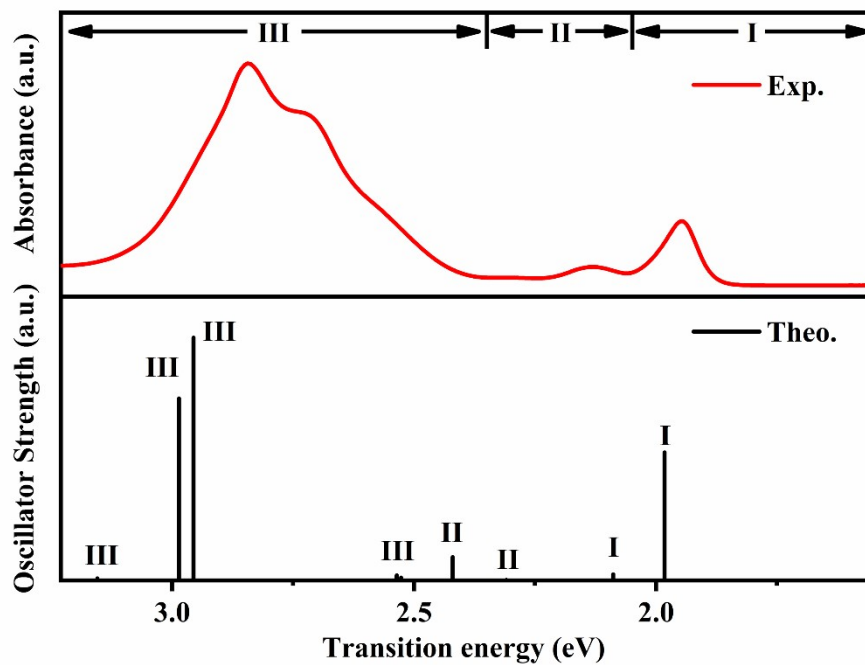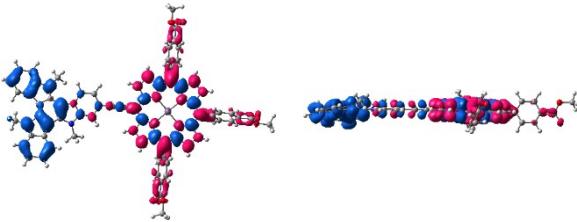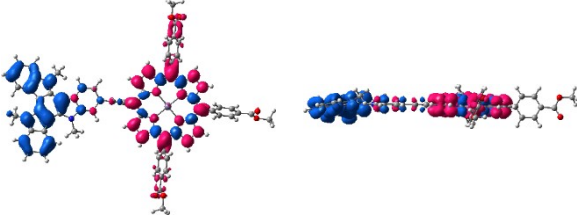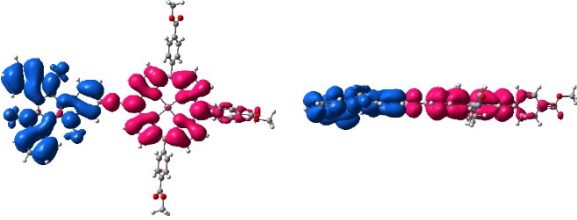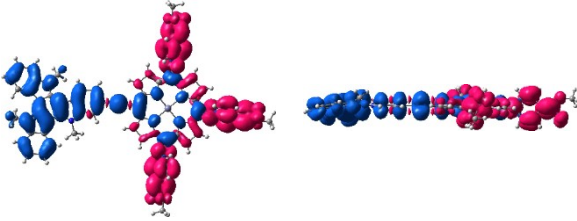
Fig. S16 The experimental and simulated electronic absorption spectra for **TAT-ZnPor**.

Table S2 Light induced electron tranfering direction (LIETD, isovalue: 2.0×10^{-4} e·au^{-3}) and light harvesting efficiency (LHE) for **TAT-ZnPor**. Electron densities move from the blue area to the red area.

| Region I		
Transition Energy: 1.98 eV **LHE：** 90.32%		**Transition:** $H-3 \rightarrow L+1(7\%)$ $H \rightarrow L(88\%)$
Transition Energy: 2.09 eV **LHE:** 10.75%		**Transition:** $H-3 \rightarrow L(22\%)$ $H-2 \rightarrow L+1(8\%)$ $H \rightarrow L+1(70\%)$
Region II		
Transition Energy: 2.31 eV **LHE:** 0.73%		**Transition:** $H-1 \rightarrow L(99\%)$
Transition Energy: 2.42 eV **LHE:** 34.55%		**Transition:** $H-3 \rightarrow L+1(27\%)$ $H-2 \rightarrow L(62\%)$ $H \rightarrow L(9\%)$
Region III		
Transition Energy: 2.53 eV **LHE:** 5.11%		**Transition:** $H-3 \rightarrow L(11\%)$ $H-2 \rightarrow L+1(16\%)$ $H-1 \rightarrow L+1(61\%)$ $H \rightarrow L+1(11\%)$
Transition Energy: 2.54 eV **LHE：** 8.80%		**Transition:** $H-3 \rightarrow L(18\%)$ $H-2 \rightarrow L+1(26\%)$ $H-1 \rightarrow L+1(38\%)$ $H \rightarrow L+1(16\%)$

Transition Energy: 2.96eV **LHE:** 98.81%		**Transition:** $H-3 \to L+1(54\%)$ $H-2 \to L(31\%)$ $H \to L+5(6\%)$
Transition Energy: 2.99 eV **LHE:** 96.39%		**Transition:** $H-3 \to L(46\%)$ $H-2 \to L+1(49\%)$
Transition Energy: 3.15 eV **LHE:** 3.59%		**Transition:** $H-4 \to L(96\%)$
Transition Energy: 3.23 eV **LHE:** 1.82%		**Transition:** $H-2 \to L+3(6\%)$ $H \to L+3(86\%)$

7. Viscosity response
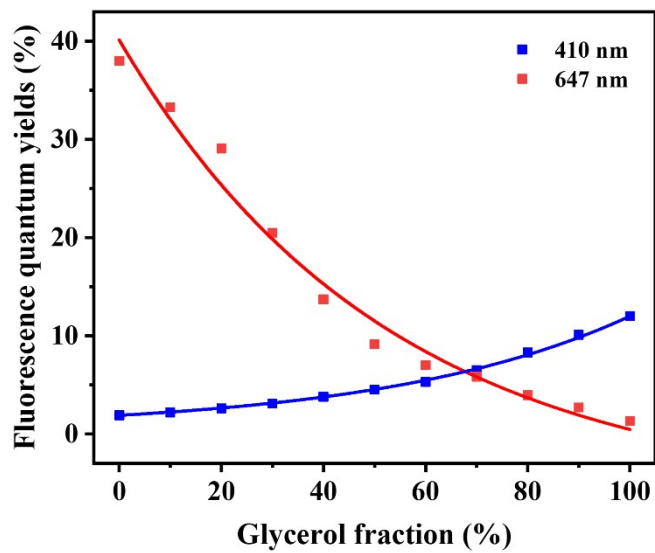
Fig. S17 Fluorescence quantum efficiencies of **TAT-ZnPor** at 410 and 647 nm in methanol/glycerol mixtures.
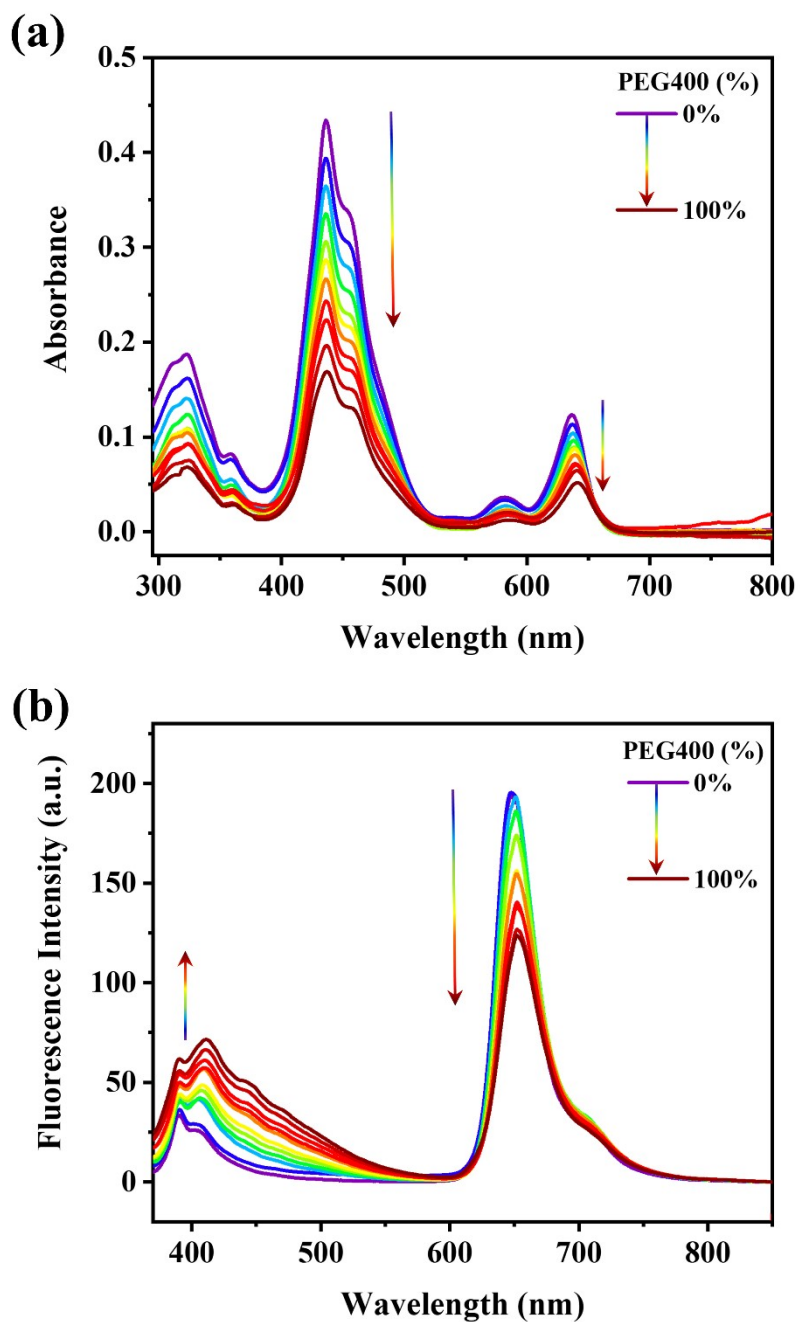
Fig. S18 (a) Absorption and (b) Fluorescence emission spectra of **TAT-ZnPor** in THF/PEG400 mixtures (1 μM, λ_{ex} = 350 nm, 0-100% PEG400).
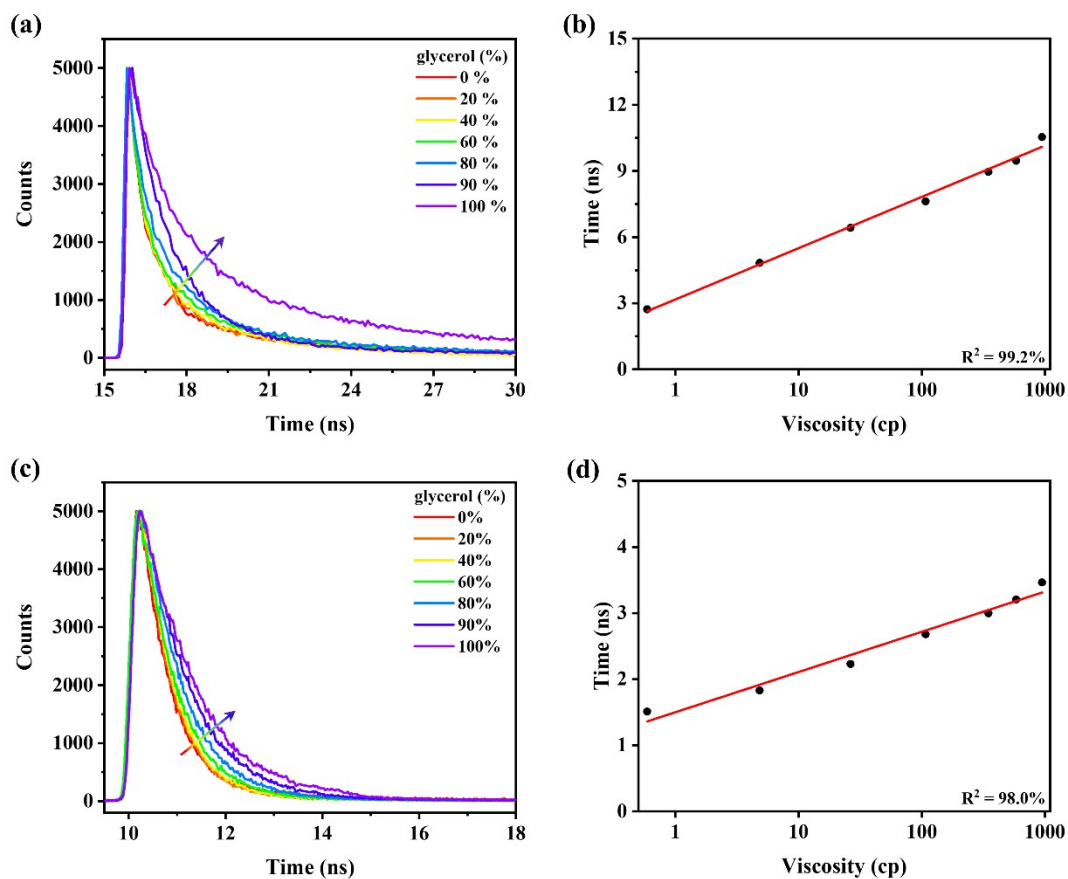
Fig. S19 Fluorescence decay curves of **TAT-ZnPor** (1 μM) at (a) 410 and (c) 647 nm in methanol/glycerol mixtures determined with excitation at 375 nm by a EPL laser; Linear relationship between fluorescence lifetime and solvent viscosity at (b) 410 and (d) 647 nm.

8. MTT Assay and Fluorescence Microscopy Images
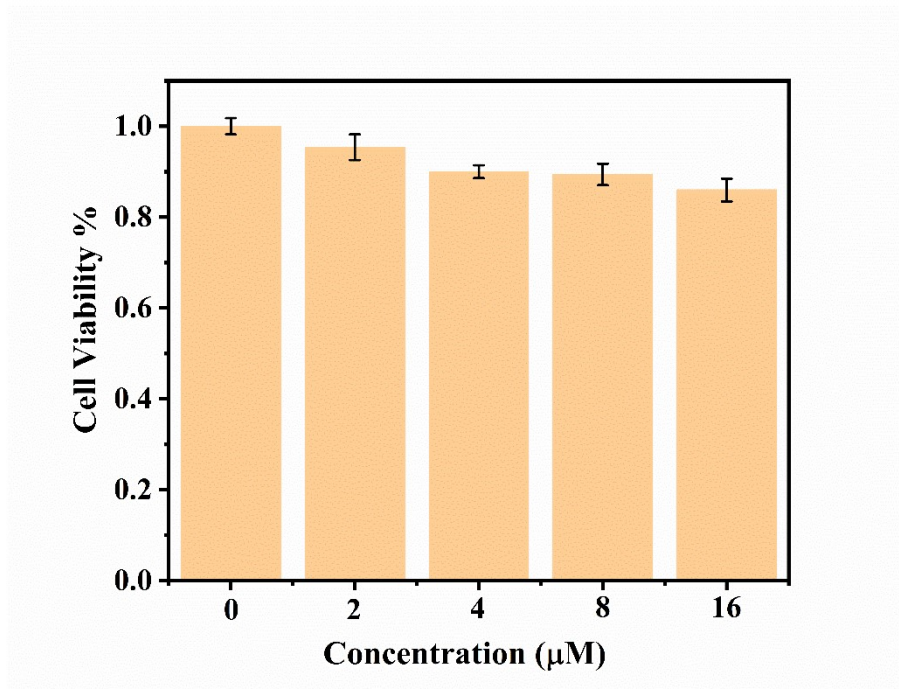
Fig. S20 Cell viability (%) estimated by a MTT assay after incubation in different concentration of **TAT-ZnPor** (0-16 μM) at 37 °C for 24 h.
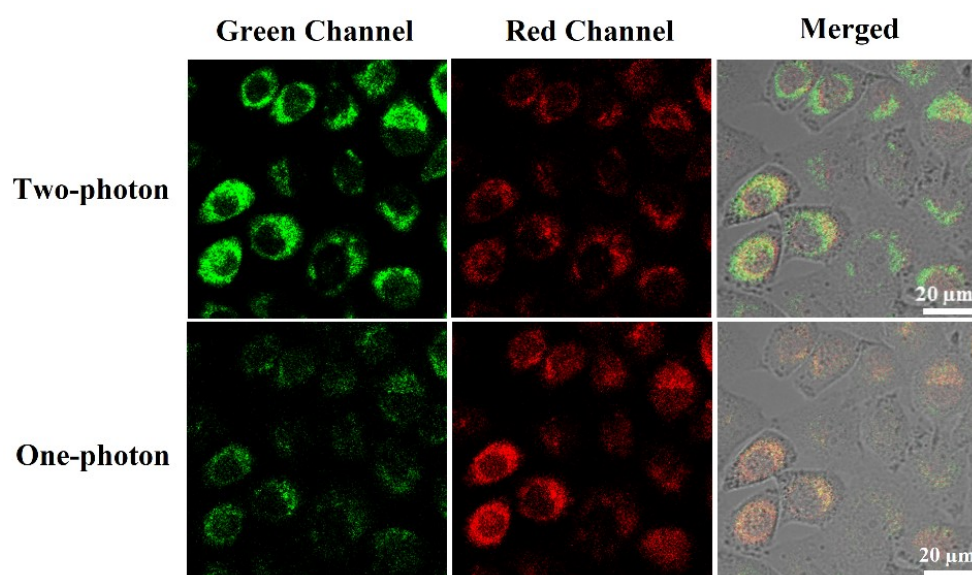
Fig. S21 Two-photon (λ_{ex} = 820 nm) and one photon (red channel, λ_{ex} = 405 nm, λ_{em} = 570-620 nm; green channel, λ_{ex} = 457 nm, λ_{em} = 500-550 nm) confocal images of A549 cells treated with 2 μM of **TAT-ZnPor**. (The last column is the merged images of bright-field, red channel and green channel.) Scale bar: 20 μm.

	Commercial dyes	Green Channel	Red Channel	Merged Channel	Bright Field	Pearson's correlation	Intensity Variations
TAT-ZnPor + Mito Tracker	(a)	(b)	(c)	(d)	(e)	(f)	(g)
TAT-ZnPor + Lyso Tracker							
TAT-ZnPor + DiI							
TAT-ZnPor + ER Tracker							
TAT-ZnPor + ActinBlue							
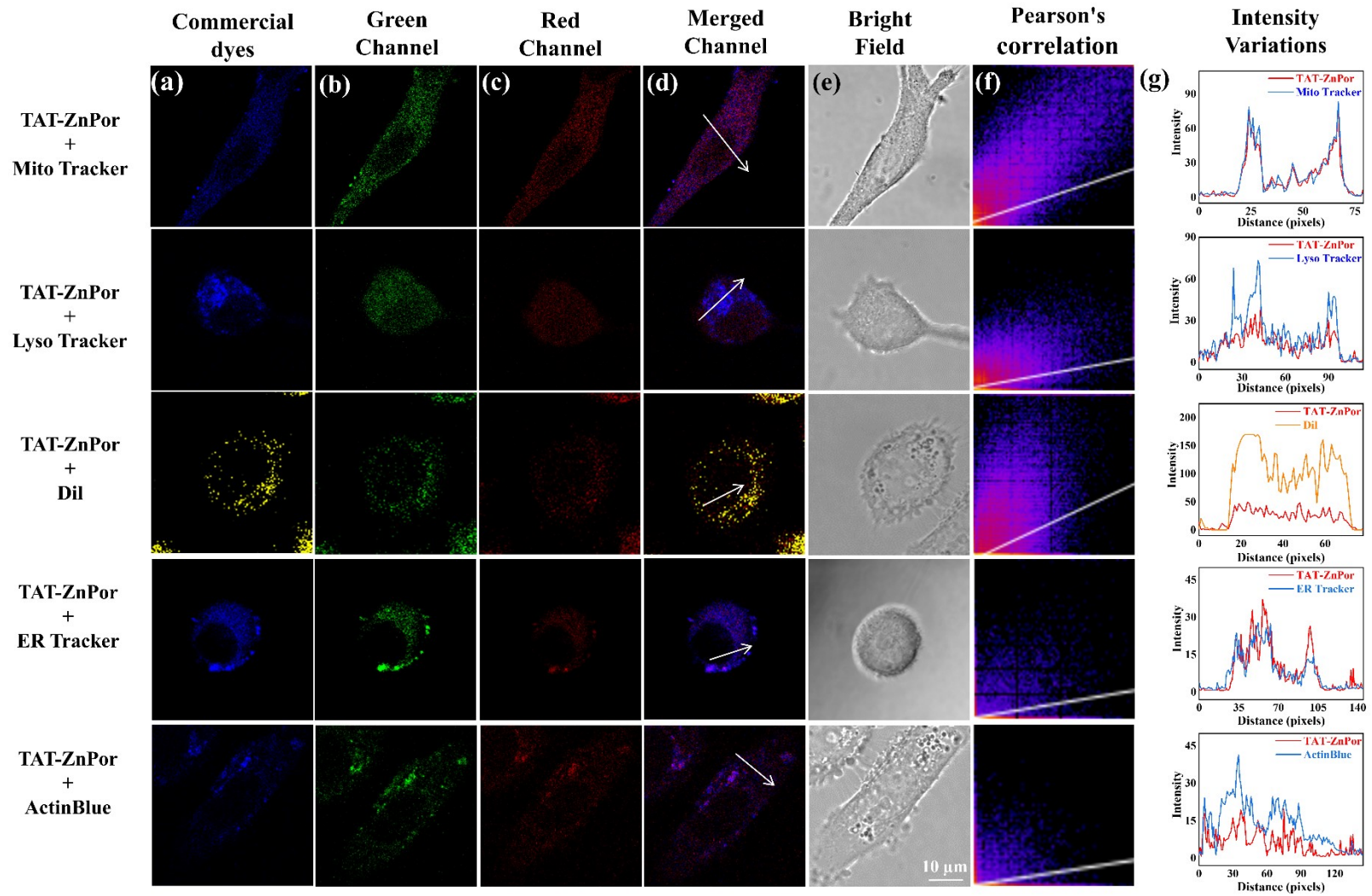
Fig. S22 Co-localization images of A549 cells for **TAT-ZnPor**. (a) Orange channel (λ_{ex} = 552 nm, λ_{em} = 550-600 nm): staining with DilC18(3) (1 μM), Blue Channel (λ_{ex} = 405 nm, λ_{em} = 400-500 nm): staining with MitoTracker Blue FX 490 (20 μM), LysoTracker Blue DND-22 (100 nM), ER-tracker Blue-White DPX (100 nM) or ActinBlue (50 U/mL); (b) Green Channel (λ_{ex} = 405 nm, λ_{em} = 500-550 nm): staining with **TAT-ZnPor** (2 μM); (c) Red Channel (λ_{ex} = 405 nm, λ_{em} = 550-700 nm): staining with **TAT-ZnPor** (2 μM); (d) Merged: the overlaps of (a) and (c); (e) Brightfield; (f) The Pearson's correlation coefficient for the overlap between Orange/Blue channel and Red channel; (g) Fluorescence intensity profiles of **TAT-ZnPor** (in red channel) and commercial trackers (in Orange/Blue channel) traced along the linear regions of interest (ROIs, bright-blue lines in (d)) across selected cells. Scale bar: 10 μm.

Table S3 Comparison of the performance of **TAT-ZnPor** with reported probes for viscosity.

Probes	$\lambda_{ex}/\lambda_{em}$	Cell localization	Detection range (cp)	Detection limit	Viscosity response coefficient	Response model	Reference
TAT-ZnPor	350/410, 647	mitochondrial	0.59-947	0.52 cp	0.29, 0.87	Ratiometric	This work
BODIPY	330/427, 516	mitochondrial	0.6-945.35	NR	NR	Ratiometric	Yang et al, *J. Am. Chem. Soc.*, 2013, **135**, 9181-9185
Qca-Cy2	335/385, 570	mitochondrial	100-950	NR	0.335	Ratiometric	Liu et al, *Tetrahedron Lett.*, 2018, **59**, 4540-4544
TM-V	425/477, 609	mitochondrial	1.01-950.2	NR	NR	Ratiometric	Ren et al, *Sensor. Actuator. B Chem.*, 2018, **262**, 452-459
porphyrin dimer **1**	453/640, 695	NR	0.6-1500	NR	NR	Ratiometric	Vyšniauskas et al, *Phys. Chem. Chem. Phys.*, 2015, **17**, 7548-7554
dABp-3	435/496, 565	NR	1.8-6.0	NR	0.69	Ratiometric	Li et al, *Anal. Chem.*, 2016, **88**, 5554-5560
RV-1@GQDs-	490/530,	NR	0-600	NR	NR	Ratiometric	Li et al, *Chem. Commun.*, 2020,

OH	635						**56**, 14649-14652
Lyso-BTC	470/685	lysosomal	0-99% Gly	NR	NR	Turn on	Chen et al, *Org. Biomol. Chem.*, 2019, **17**, 6398-6403
MCB	420/566	mitochondrial	0.59-945.5	NR	0.43	Turn on	Fang et al, *Sensor. Actuator. B Chem.*, 2019, **297**, 126777
VPZ1-3	-/515	NR	20-80% Gly	NR	NR	Turn on	Lei et al, *Front. Chem.*, 2019, **7**, 342
H-V	400/520	cytoplasmic	0.59-945	NR	0.50	Turn on	Li et al, *J. Am. Chem. Soc.*, 2019, **141**, 18301-18307
RFC-MRC	405/600	mitochondrial	NR	NR	NR	Turn on	He et al, *Anal. Chem.*, 2019, **91**, 15220-15228
CBI-V	520/610	mitochondrial	1.4-956	NR	0.52	Turn on	Yin et al, *Anal. Chem.*, 2019, **91**, 8415-8421
NI-VIS	560/670	mitochondrial	1-999	NR	0.96	Turn on	Zhang et al, *Anal. Chem.*, 2019, **91**, 10302-10309
BMVC	470/550	mitochondrial	0.893-435	NR	0.54	Turn on	Zou et al, *Anal. Chem.*, 2019, **91**, 8574-8581
BV-1	545/570	mitochondrial	2-868	0.16 cp	0.47	Turn on	Sun et al, *Talanta*, 2021, **225**, 121996

Lyso-B	550/586	lysosomal	1-1410	NR	NR	Turn on	Li et al, *Anal. Chem.*, 2018, **90**, 5873-5878
Lyso-BTC	505/685	lysosomal	0-99% Gly	NR	NR	Turn on	Chen et al, *Org. Biomol. Chem.*, 2019, **17**, 6398-6403
BTV	470/520	mitochondrial	0.6-950	NR	0.72	Turn on	Su et al, *Sensors*, 2016, **16**, 1397
Mito-V	561/634	mitochondrial	1.7-953	NR	NR	Turn on	Peng et al, *New J. Chem.*, 2019, **43**, 16945-16949
MHC-V1 MHC-V2	470/628 545/579	mitochondrial	3.2-317	NR	NR	Turn on	Zhou et al, *New J. Chem.*, 2017, **41**, 11507-11511
RM-V	530/575	mitochondrial	2.1-1596	NR	NR	Turn on	Dai et al, *Anal. Methods*, 2019, **11**, 4561-4565
NI-VIS	560/670	mitochondrial	1.0-999	NR	0.96	Turn on	Zhang et al, *Anal. Chem.*, 2019, **91**, 10302-10309
RV-1	573/655	mitochondrial	0.6-953	NR	0.58	Turn on	Guo et al, *J. Mater. Chem. B*, 2018, **6**, 2894-2900
TPSN	525/637	mitochondrial	1-950	NR	0.646	Turn on	Wang et al, *Chem. Pap.*, 2020, **74**, 1071-1078
NV-1	590/744	mitochondrial	0.6-950	NR	0.40	Turn on	Guo et al, *Talanta*, 2019, **204**, 868-874

NL1	473/594	mitochondrial	0-90% Gly	NR	NR	Turn on	Tian et al, *Dyes Pigm.*, 2017, **147**, 90-98
NL2	478/593						
NL3	470/592						
PL1	472/594	mitochondrial	0-90% Gly	NR	NR	Turn on	Tian et al, *Dyes Pigm.*, 2017, **147**, 90-98
PL2	476/595						
PL3	470/591						
MitoSN	420/520	mitochondrial	1.0-950	NR	0.495	Turn on	Wang et al, *Spectrochim. Acta. Part A*, 2018, **203**, 127-131
TDHC	525/592	mitochondrial	0-453	NR	0.59	Turn on	Baek et al, *Biosens. Bioelectron.*, 2016, **86**, 885-891
L	515/590	mitochondrial	0-99% Gly	NR	NR	Turn on	Wang et al, *New J. Chem.*, 2019, **43**, 8811-8815
SFC-Cy007	678/697	mitochondrial	1-621	NR	NR	Turn on	Park et al, *Dyes Pigm.*, 2020, **174**, 108080
PFV	525/570	mitochondrial	1-1412	NR	NR	Turn on	Wu et al, *Dyes Pigm.*, 2019, **168**, 134-139
Mito-V	511/583	mitochondrial	0-100% Gly	NR	0.58	Turn on	Chen et al, *Chem. Commun.*, 2019, **55**, 7410-7413
Vis-A	501/517	mitochondrial	0.6-360	NR	NR	Turn on	Song et al, *J. Mater. Chem. B*,

								2017, **5**, 360-368
HC-1	610	mitochondrial	13.5-950	NR	0.457	Turn on		Raja et al, *Chemistry Select*, 2017, **2**, 4609-4616
TPE-V	460/650	mitochondrial	1.4-950	NR	0.674	Turn on		Ma et al, *J. Mater. Chem. B*, 2018, **6**, 6212-6216
MitoAIE1	-/625	mitochondrial	0.89-942.5	NR	0.38	Turn on		Chen et al, *Anal. Chem.*, 2018, **90**, 8736-8741
LysoAIE1	-/540	lysosomal	0.89-942.5	NR	0.32	Turn on		Chen et al, *Anal. Chem.*, 2018, **90**, 8736-8741
Mito-VS	500/610	mitochondrial	1.03-584.5	NR	NR	Turn on		Li et al, *Anal. Chem.*, 2018, **90**, 94189425
CBI-V	520/610	mitochondrial	1.4-956	NR	0.524	Turn on		Yin et al, *Anal. Chem.*, 2019, **91**, 8415-8421
EIMV	510/600	mitochondrial	1.5-1099.5	NR	NR	Turn on		Wang et al, *Analyst*, 2019, **144**, 6247-6253
NV	580/635	mitochondrial	0-95% Gly	NR	0.453	Turn on		Zhu et al, *Dyes Pigm.*, 2020, **172**, 107859
BMVC	470/560	mitochondrial	0.893-435	NR	NR	Turn on		Zou et al, *Anal. Chem.*, 2019, **91**, 8574−8581

FMR-1 FMR-2	460/525	mitochondrial	0.6-1178	NR	NR	Turn on	Steinmark et al, *PLoS One*, 2019, **14**, e0211165
Mito-VH	500/610	mitochondrial	Ethanol-Gly	NR	NR	Turn on	Ren et al, *Anal. Chem.*, 2017, **89**, 552-555
Mito-LX	480/730	mitochondrial	0.60-945	NR	0.44	Turn on	Li et al, *J. Mater. Chem. B*, 2019, **7**, 4243-4251
TP-1Bz	340/403, 650	mitochondrial	103.0-95.5	NR	NR	Turn on	Sun et al, *Sensor. Actuator. B Chem.*, 2018, **276**, 238-246
MBCB	351/415, 567	mitochondrial	0.99-1396	NR	0.23	Turn on	Sun et al, *Dyes Pigm.*, 2019, **171**, 107709
BODIPY-2	485/510	NR	0.6-930	NR	NR	Turn on	López-Duarte et al, *Chem.Commun.*, 2014, **50**, 5282-5284
1b	546/648	endoplasmic reticulum	0.89-856	NR	1.31	Turn on	Wang et al, *J. Mater. Chem. B*, 2021, **9**, 5664-5669
TbL[1]	310/542	NR	1.8-6.0	NR	0.18	Turn on	Bui et al, *J. Am. Chem. Soc.*, 2017, **139**, 7693-7696
BDP-V BG	490/520	NR	0.6-248	NR	0.018	Turn on	Wang et al, *Biosens. Bioelectron.*, 2017, **89**, 757-764

Lyso-NA	550/610	lysosomal	1-1410	NR	NR	Turn on	Guo et al, *J. Mater. Chem. B*, 2018, **6**, 580-585
BTP	590/635	lysosomal	0.96-965	NR	NR	Turn on	Ren et al, *J. Mater. Chem. B*, 2019, **7**, 6181-6186
DXB-CBT	560/614	NR	0.6-1317	NR	0.61	Turn on	Karpenko et al, *J. Mater. Chem. C*, 2016, **4**, 3002-3009
BDHA	457/539	lysosomal	1.62-851.6	NR	0.63	Turn on	Chen et al, *Spectrochim. Acta, Part A*, 2022, **175**, 121141
VLAP	550/700	mitochondrial	0.893-435	NR	0.65	Turn on	Li et al, *Chem. Eng. J.*, 2022, **435**, 135043
Lys-V	430/515	lysosomal	7.9-438.4	NR	NR	Turn on	Li et al, *J. Mater. Chem. B*, 2018, **6**, 6592-6598
MCN	400/470	cytoplasm	1.03-956	NR	0.65	Turn on	Ning et al, *J. Mater. Chem. B*, 2017, **5**, 2743-2749

NR: Not Reported.

9. References

1 N. S. Makarov, M. Drobizhev and A. Rebane, *J. Opt. Soc. Am. B*, 2008, **16**, 4029-4047.

2 C. Xu and W. W. Webb, *J. Opt. Soc. Am. B*, 1996, **13**, 481-491.

3 (a) R. Bauernschmitt and R. Ahlrichs, *Chem. Phys. Lett.*, 1996, **256**, 454-464; (b)M. E. Casida, C. Jamorski, K. C. Casida and D. R. Salahub, *J. Chem. Phys.*, 1998, **108**, 4439-4449; (c) R. E. Stratmann, G. E. Scuseria and M. J. Frisch, *Chem. Phys. Lett.*, 1996, **257**, 213-233; (d) C. V. Caillie and R. D. Amos, *Chem. Phys. Lett.*, 1999, **308**, 249-255; (e) C. V. Caillie and R. D. Amos, *Chem. Phys. Lett.*, 2000, **317**, 159-164; (f) F. Furche and R. Ahlrichs, *J. Chem. Phys.*, 2002, **117**, 7433-7447; (g) G. Scalmani, M. J. Frisch, B. Mennucci, J. Tomasi, R. Cammi and V. Barone, *J. Chem. Phys.*, 2006, **124**, 1-15.

4 (a) J. P. Perdew, K. Burke and M. Ernzerhof, *Phys. Rev. Lett.*, 1996, **77**, 3865-3868; (b) J. P. Perdew, K. Burke and M. Ernzerhof, *Phys. Rev. Lett.*, 1997, **78**, 1396; (c) C. Adamo and V. Barone, *J. Chem. Phys.*, 1999, **110**, 6158-6170.

5 M. J. Frisch, G. W. Trucks, H. B. Schlegel, G. E. Scuseria, M. A. Robb, J. R. Cheeseman, G. Scalmani, V. Barone, B. Mennucci, G. A. Petersson, H. Nakatsuji, M. Caricato, X. Li, H. P. Hratchian, A. F. Izmaylov, J. Bloino, G. Zheng, J. L. Sonnenberg, M. Hada, M. Ehara, K. Toyota, R. Fukuda, J. Hasegawa, M. Ishida, T. Nakajima, Y. Honda, O. Kitao, H. Nakai, T. Vreven, J. A. Montgomery Jr., J. E. Peralta, F. Ogliaro, M. J. Bearpark, J. Heyd, E. N. Brothers, K. N. Kudin, V. N. Staroverov, R. Kobayashi, J. Normand, K. Raghavachari, A. P. Rendell, J. C. Burant, S. S. Iyengar, J. Tomasi, M. Cossi, N. Rega, N. J. Millam, M. Klene, J. E. Knox, J. B. Cross, V. Bakken, C. Adamo, J. Jaramillo, R. Gomperts, R. E. Stratmann, O. Yazyev, A. J. Austin, R. Cammi, C. Pomelli, J. W. Ochterski, R. L. Martin, K. Morokuma, V. G. Zakrzewski, G. A. Voth, P. Salvador, J. J. Dannenberg, S. Dapprich, A. D. Daniels, Ö. Farkas, J. B. Foresman, J. V. Ortiz, J. Cioslowski, and D. J. Fox, Gaussian, Inc, Wallingford, CT, USA, 2009.

6 (a) R. B. J. S. Krishnan, J. S. Binkley, R. Seeger and J. A. Pople, *J. Chem. Phys.*, 1980, **72**, 650-654; (b) M. Dolg, U. Wedig, H. Stoll and H. Preuss, *J. Chem. Phys.*, 1987, **86**, 866-872; (c) J. M. Martin and A. Sundermann, *J. Chem. Phys.*, 2001, **114**, 3408-3420.

7   G. Scalmani and M. J. Frisch, *J. Chem. Phys.*, 2010, **132**, 114110.

8   (a) T. Lu and F. Chen, *J. Comput. Chem.*, 2012, **33**, 580-592; (b) T. Lu, Q. Chen, *Theor. Chem. Acc.*, 2020, **139**, 25; (c) W. Humphrey, A.Dalke and K. Schulten, *J. Mol. Graph.*, 1996, **14**, 33-38.

9   D. D. Qi, TD-Analy (Version 1.13), University of Science and Technology Beijing, Beijing, China, 2015.

10 H. Maeda, T. Maeda, K. Mizuno, K. Fujimoto, H. Shimizu and M. Inouye, *Chem. Eur. J.*, 2006, **12**, 824-831.

11 D. J. Quimby and F. R. Longo, *J. Am. Chem. Soc.*, 1975, **97**, 5111-5117.